Experimental Heat Transfer, 23:27–43, 2010

ISSN: 0891-6152 print/1521-0480 online
DOI: 10.1080/08916150903402724

Taylor & Francis
Taylor & Francis Group

EFFECT OF VELOCITY DISTRIBUTION ON EXTERNAL WALL TEMPERATURE FIELD FOR A FLAT MICROCHANNEL

I. Perry,[1] Y. Jannot,[1] D. Maillet,[1] and B. Fiers[1,2]
[1]*Laboratoire d'Energétique et de Mécanique Théorique et Appliquée (LEMTA), Nancy Université and CNRS, Vandoeuvre-Lès Nancy, France*
[2]*Institut Français du Pétrole Lyon, Solaize, France*

Experimental temperature distributions on the external walls of a heated flat microchannel contain information on the temperature and velocity fields in the cross-section of the dynamically developed internal flow. The relationship between the heat source surface distribution on the external wall and the temperature field on the same or opposite face is derived using Fourier transforms of the temperature distribution in the direction of the water flow. The corresponding transfer function depends analytically on the velocity distribution. A sensitivity analysis of the temperature distribution to the velocity profile is implemented for different Péclet numbers in order to design a corresponding bench.

Keywords direct and inverse problems, velocity distribution, infrared thermography, microchannel heat transfer, conduction and advection, thermal quadrupoles

INTRODUCTION

Flow in microchannels for hydraulic diameters of submillimetric size is characterized by three specific effects: entrance effects, viscous dissipation, and axial heat conduction through the walls [1]. This last effect is associated to a purely geometric property; in this kind of system, the solid wall cross-section has the same order of magnitude as the flow section, which makes a strong coupling appear between conduction in the walls and associated conduction and advection in the flow [2, 3]. Because of this strong contribution of the solid phase to heat transfer, it may be pertinent to consider microchannels or larger systems made of a combination of these, such as compact heat exchangers, as porous materials submitted to thermal dispersion [4].

The focus here is on the problem of the possible measurement of the velocity and temperature distributions in the section of a heated microchannel. It is a difficult task for several reasons. Local probes can modify both heat transfer and local velocities because the small dimensions involved (intrusive measurements) and use of optical techniques can be affected by the presence of the walls. The use of another class of technique, an inverse conduction/convection method, can be considered. This class of technique consists of measuring the temperature distribution on some part of the system and comparing it to its theoretical counterpart (the model) in order to estimate the velocity and temperature fields in a situation where heat transfer is the result of both conduction and advection.

Received 20 February 2009; accepted 30 March 2009.
Address correspondence to Isabelle Perry, LEMTA, Nancy Université and CNRS, Vandoeuvre-lès-Nancy, Cedex, 54504, France. E-mail: isabelle.perry@ensem.inpl-nancy.fr

NOMENCLATURE

a	thermal diffusivity ($m^2.s^{-1}$)
c	thermal capacity ($J.kg^{-1}.K^{-1}$)
e	thickness (m)
F	quadrupolar matrix of fluid
h	heat transfer coefficient ($W.m^{-2}.K^{-1}$)
H	quadrupolar matrix for external convection transfer
K	number of fluid layers
L	microchannel length (m)
N	number of harmonics
Pe	Péclet number
Pr	Prandtl number
Q	heat flux density ($W.m^{-2}$)
Re	Reynolds number
S	quadrupolar matrix of solid walls
T	temperature (K)
u	velocity ($m.s^{-1}$)
U	mean velocity ($m.s^{-1}$)
w	width (m)
X	reduced sensitivity (K)

Greek Letters

α	Fourier variable (m^{-1})
λ	thermal conductivity ($W.m^{-1}.K^{-1}$)
ν	kinematic viscosity ($m^2.s^{-1}$)
ρ	density ($kg.m^{-3}$)
Φ	heat flux (W)

Subscripts

f	fluid
f	front face
i	solid wall number or imaginary unit number
k	fluid layer number
n	harmonics number (integer)
r	rear face
s	solid
∞	external conditions (air)

Superscripts

$\sim$	Fourier transform

DIRECT PROBLEM AND MODEL

A three-layer structure, composed of a channel between two parallel walls and of very large length ($2L$), is considered here (Figure 1). The flow is supposed to be fully, dynamically developed with a velocity distribution $u(y)$.

The two solids (subscript $\omega = s$) and the fluid (subscript $\omega = f$) media are characterized by thicknesses e_ω, conductivities λ_ω, and volumetric heat capacities ρc_ω. The (front) face is stimulated with a surface heat source whose space distribution is composed of two door functions of equal length and of equal intensities (positive then negative) Φ (in W). Heat losses (convection and linearized radiation) with the ambient environment at temperature $T_\infty = 0$ are characterized by a uniform h coefficient.

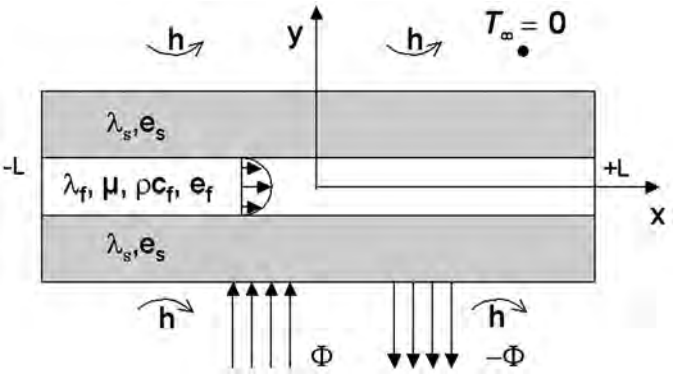

Figure 1. Geometry and structure of the flow.

The heat equations in the walls (lower heated wall, subscript 1; upper wall, subscript 2), as well as the axial boundary conditions are

$$\frac{\partial^2 T_i}{\partial x^2} + \frac{\partial^2 T_i}{\partial y^2} = 0 \quad (\text{for } i = 1, 2);\ T_i \to 0 \text{ as } x \to \pm\infty. \tag{1}$$

The heat equation in the fluid as well as its axial boundary conditions can be written as

$$\lambda_f \left(\frac{\partial^2 T_f}{\partial x^2} + \frac{\partial^2 T_f}{\partial y^2} \right) - \rho c_f u(y) \frac{\partial T_f}{\partial x} = 0; \qquad T_f \to 0 \text{ as } x \to \pm\infty. \tag{2}$$

Transverse conditions on external boundaries are

$$\begin{aligned} -\lambda_s \frac{\partial T_1}{\partial y} &= -h(T_1 - T_\infty) + q(x) \quad \text{at} \quad y = -\frac{e_f}{2} - e_s; \\ -\lambda_s \frac{\partial T_2}{\partial y} &= h(T_2 - T_\infty) \quad \text{at} \quad y = \frac{e_f}{2} + e_s, \end{aligned} \tag{3}$$

where $q(x)$ is the heating power surface density. Solid/fluid interface conditions are

$$-\lambda_s \frac{\partial T_i}{\partial y} = -\lambda_f \frac{\partial T_f}{\partial y} \quad \text{and } T_i = T_f \text{ (for } i = 1, 2) \text{ at } y = \pm\frac{e_f}{2}. \tag{4}$$

The velocity field $u(y)$ within the flow can be made homogeneous through the discretization of the fluid layer into K fluid layers of thicknesses $e_k = y_k - y_{k-1} = e_f/K$, with $y_0 = -e_f/2$ (see Figure 2).

This discretization transforms this field into K velocities u_k that constitute thermophysical parameters playing the same role as conductivity λ_f or volumetric heat ρc_f of the heat transfer problem.

The Fourier transform of temperature T can be written as

$$\tilde{T}(\alpha, y) = \int_{-\infty}^{+\infty} T(x, y) e^{-i\alpha x} dx \quad (\text{length } L = +\infty).$$

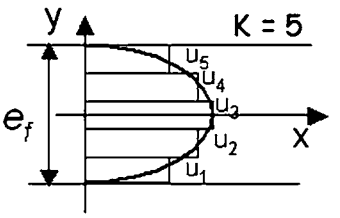

Exact velocity distribution :

$$u(y) = \frac{3}{2} U \left[1 - 4 (y/e_f)^2 \right]$$

Parameterized velocity distribution :

$$u_k = \frac{3}{2} U \left[1 - \frac{4K}{3e_f^3} \left(y_k^3 - y_{k-1}^3 \right) \right]$$

U: mean velocity

Discretization of $u(y)$ into a piecewise constant function with $K = 5$ parameters

Figure 2. Parameterization of the velocity distribution—case of a laminar flow with five layers.

This transform exists only if the integral of the square of temperature T over the channel length (the square of the norm of function T of the x variable for a fixed value of y) is finite; the selected axial boundary conditions in Eqs. (1) and (2) hence correspond to a zero global heating (the integral of $q(x)$ over the channel length is equal to zero). In practice, the channel length $2L$ is finite and discrete eigenvalues α_n that correspond to this finite support are used:

$$\tilde{T}(\alpha_n, y) = \tilde{T}_n(y) = \int_{-L}^{+L} T(x, y) e^{-i\alpha_n x} dx \quad \text{with } \alpha_n = \frac{n\pi}{L}. \tag{5}$$

The Fourier inversion of Eq. (5) requires a truncation to a $(2N+1)$ number of harmonics:

$$T(x, y) = \frac{1}{2L} \sum_{n=-\infty}^{\infty} \tilde{T}_n(y) e^{-i\alpha_n x} \approx \frac{1}{2L} \sum_{n=-N+1}^{N} \tilde{T}_n(y) e^{-i\alpha_n x}. \tag{6}$$

Finite Fourier transformation of heat Eqs. (1) and (2) can be implemented as

$$\frac{d^2\tilde{T}_n}{dy^2} - \alpha_n^2 \tilde{T}_n = 0, \qquad \frac{d^2\tilde{T}_n}{dy^2} - \gamma_{nk}^2 \tilde{T}_n = 0, \quad \text{with} \quad \gamma_{nk}^2 = \alpha_n^2 + i\frac{u_k}{a_f}\alpha_n. \tag{7}$$

The transverse boundary and interface conditions in Eqs. (3) and (4) are also transformed, which means that temperature $T(x, y)$ is replaced by its transforms $\tilde{T}_n(y)$. It is further assumed that the temperature of the environment T_∞ is equal to the inlet fluid temperature (taken as zero here).

Using the Fourier transform of the transverse conduction heat flux $\tilde{\varphi}_n(y) = -\lambda_\omega d\tilde{T}_n/dy$ in each medium ($\omega = s$ or f), Eqs. (1) to (5) can be written under a quadrupolar form [5] as

$$\begin{bmatrix} \tilde{T}_{Fn} \\ \tilde{q}_n \end{bmatrix} = \mathbf{H}_1 \mathbf{S}_n \left(\prod_{k=1}^{K} (\mathbf{F}_{kn}) \right) \mathbf{S}_n \mathbf{H}_2 \begin{bmatrix} \tilde{T}_{\mathrm{AR}n} \\ 0 \end{bmatrix} = \begin{bmatrix} A_n & B_n \\ C_n & D_n \end{bmatrix} \begin{bmatrix} \tilde{T}_{\mathrm{R}n} \\ 0 \end{bmatrix}, \tag{8}$$

with

$$\mathbf{H}_1 = \mathbf{H}_2 = \begin{bmatrix} 1 & 0 \\ h & 1 \end{bmatrix}, \qquad \mathbf{S}_n = \begin{bmatrix} A_n & B_n \\ C_n & A_n \end{bmatrix}, \qquad \mathbf{F}_{kn} = \begin{bmatrix} A_{kn} & B_{kn} \\ C_{kn} & A_{kn} \end{bmatrix}, \tag{9}$$

$$\text{and} \quad \begin{matrix} T_F = T(x, -e_s - e_f/2) \\ T_R = T(x, e_s + e_f/2) \end{matrix};$$

and

$$A_n = \cosh(\alpha_n e_s), \qquad B_n = \sinh(\alpha_n e_s)/(\lambda_s \alpha_n), \qquad C_n = \lambda_s \alpha_n \sinh(\alpha_n e_s),$$

$$A_{kn} = \cosh(\gamma_{kn} e_k), \qquad B_{kn} = \sinh(\gamma_{kn} e_k)/(\lambda_f \gamma_{kn}), \qquad C_{kn} = \lambda_f \gamma_{kn} \sinh(\gamma_{kn} e_k). \tag{10}$$

SIMULATIONS AND SENSITIVITIES

Front and Rear Face Temperature Distributions

The walls and channel thicknesses are supposed to be equal ($e_s = e_f = 1$ mm), with a wall conductivity $\lambda_s = 0.2$ $\mathrm{Wm^{-1}K^{-1}}$ with water as a flowing fluid ($\lambda_f = 0.63$ $\mathrm{Wm^{-1}K^{-1}}$, $\rho c_f = 4.18\ 10^6$ $\mathrm{Jm^{-3}K^{-1}}$, kinematic viscosity $\nu = 10^{-6}$ $\mathrm{m^2/s}$). Here, a mean velocity $U = 1$ mm/s (Reynolds number $\mathrm{Re} = 2e_f U/\nu = 2$) corresponding to a parabolic velocity distribution is considered (see Figure 2). The double positive then negative power excitation (see Figure 1) corresponds to a power (electrical and consequently thermal) Φ over two equal lengths $L_{source} = 50$ mm, the gap between the two sources being equal $L_{gap} = 30L_{source}$. Under these conditions, the distance between the two sources is large enough to make the transverse temperature distribution created by the first positive source relax before the second negative source.

A length $L = 2$ m is used for the direct and inverse Fourier transforms, and $N = 8{,}000$ harmonics are used. Successive use of Eqs. (8) and (6) allows the calculation of axial temperature distributions for any ordinate y in the channel or in its walls. External heat losses are characterized by a heat transfer coefficient $h = 10$ $\mathrm{Wm^{-2}K^{-1}}$. Distributions of temperature over the external faces of the walls (the front T_F and rear face T_R temperatures) are shown in Figure 3 for a uniform power density $q = \Phi/(L_{source}w) = 4{,}000$ $\mathrm{W/m^2}$, w being the width of the source and system in the third dimension. It corresponds to a discretization of the velocity distribution into $K = 3$ pieces.

This shows that the previous choice for the different lengths allows the extraction of the axial temperature distribution over the length L_{source} of the first source from the global distribution over the total length $2L$. With this choice of lengths, the dimensionless number that assesses the importance of axial conduction effect, that is, the ratio of the fluxes transferred by axial conduction in the wall and by fluid advection (see [2, 3]), is $M = \lambda_s e_s/(\rho c_f e_f L_{source} U) \approx 10^{-3} \ll 1$; this means that the wall/fluid transfer is

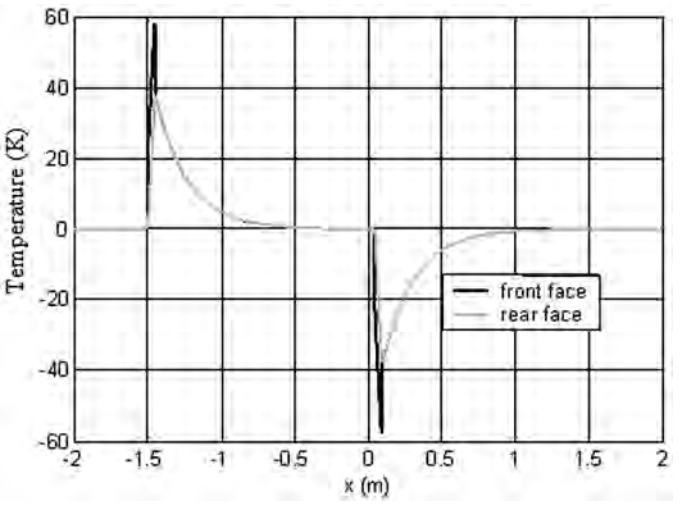

Figure 3. Global distribution of the front and rear temperatures.

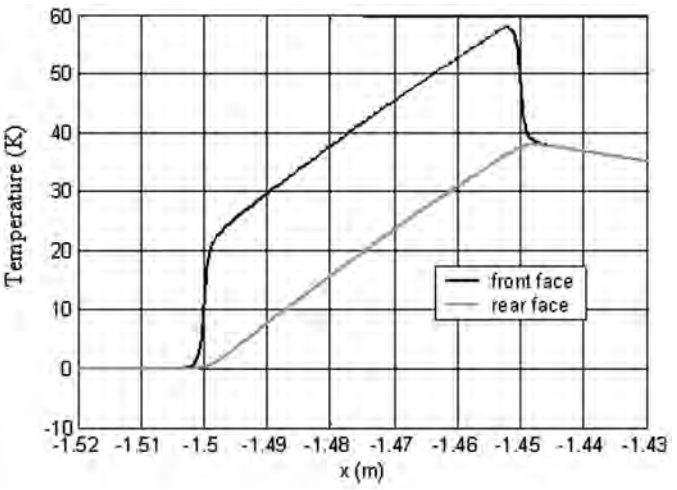

Figure 4. Local distribution of the front and rear temperatures over the heating region.

one-dimensional locally. A zoom on the front and rear face temperatures over the heating region (the first source is active between $x = -1{,}500$ mm and $x = -1{,}450$ mm) is shown in Figure 4.

It can be seen in Figure 4, which corresponds to a Péclet number $\mathrm{Pe} = \mathrm{Re}\,\mathrm{Pr} = 13.3$ (where the Prandtl number $\mathrm{Pr} = \nu/a_f = 6.64$, $a_f = \lambda_f/\rho c$ being the fluid thermal diffusivity), that both rear and front face temperature distributions are mainly linear, except at the start of the heating interval, where conduction in the solid and in the fluid make both temperatures increase upstream. Another exception occurs right before the end of the heating interval, where the front face temperature starts to decrease upstream. These effects in the transition sections will be very useful for the estimation of the transverse fluid distribution (see the section entitled "Sensitivity to the Velocity Components").

Péclet Number Effect

The effect of the Péclet number can be observed in Figures 5a to 5d. For a very low velocity ($\mathrm{Pe} = 0.133$, Figure 5a), diffusion is the dominant mode of heat transfer, since the solid is quasi at rest and both temperature distributions are nearly symmetrical with respect to the section that corresponds to the center of the thermal power source. Conversely, for very high velocities ($\mathrm{Pe} = 133$, Figure 5d), axial advection is dominant, and the temperature distributions of both external faces are mainly linear. However, one can notice that the strictly linear section of these profiles is shorter in Figure 5d ($\mathrm{Pe} = 133$), with a lag in the start of the temperature rise in the rear face, in particular, than in Figure 5c ($\mathrm{Pe} = 13.3$). This comes from the fact that these Péclet numbers only assess the relative effects of *axial* advection and conduction in the fluid domain. However, transverse conduction (in both fluid and solid) is absolutely necessary to transfer heat in the direction normal to the flow. Since the heating power is the same in both cases, with lower fluid heating for the highest velocity as a consequence, the $\mathrm{Pe} = 133$ case also corresponds to a higher effect of lateral heat diffusion and a larger transition region

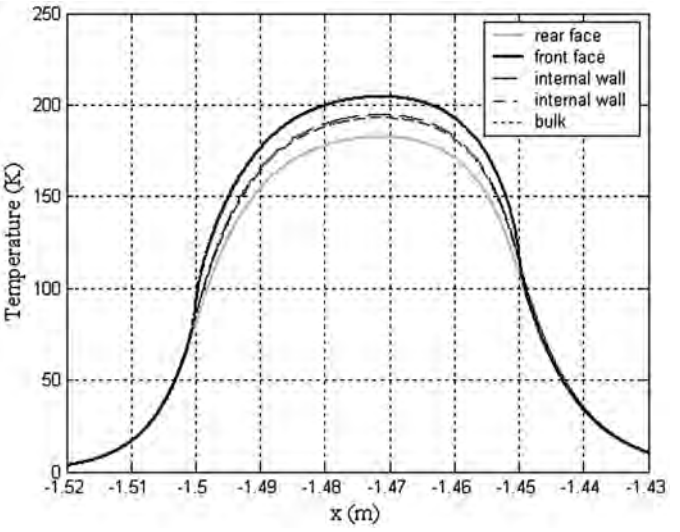

(a)

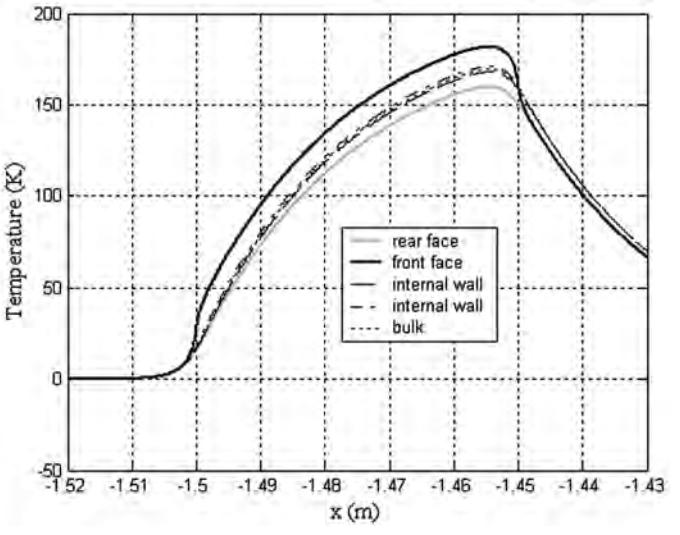

(b)

Figure 5. Effect of the Péclet number on the distribution of front and rear face temperatures, internal wall temperatures, and bulk temperature (analytical model; same excitation $q = 4{,}000\ \mathrm{Wm}^{-2}$; $L_{source} = 50$ mm; velocity distribution parameterized into $K = 3$ pieces): (a) Pe = 0.133, (b) Pe = 1.33, (c) Pe = 13.3, and (d) Pe = 133. (*continued*)

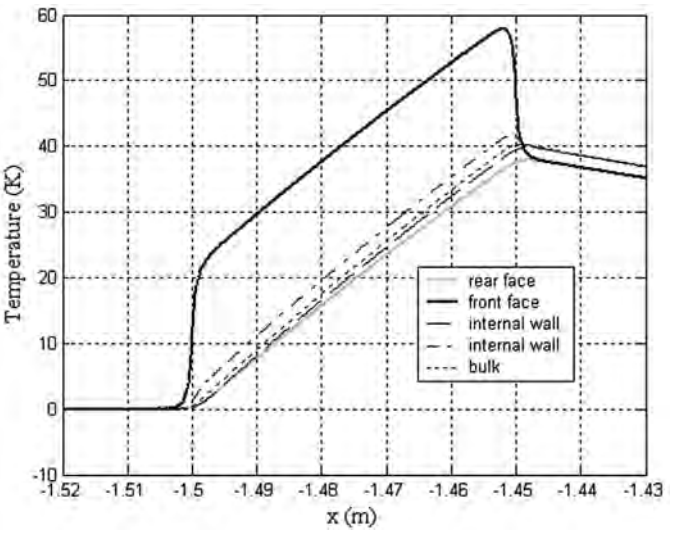

(c)

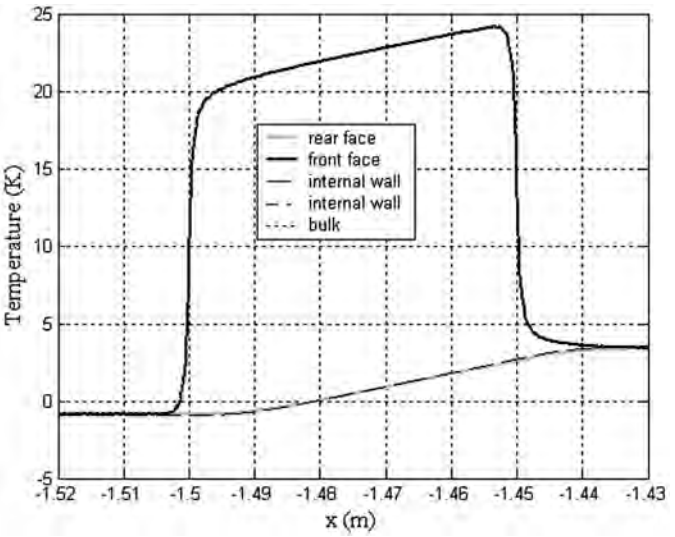

(d)

Figure 5. (*Continued*).

for both solid faces. Apart from this effect, one can notice a continuous transition of the temperature profiles with the variation of the Péclet number in Figures 5a to 5d.

The temperature distributions shown in Figure 5 and derived from the analytical model have been compared with the corresponding output of the finite volume code COMSOL® (COMSOL France, Paris, France) for exactly the same input parameters. The distributions of the front and rear face temperatures calculated by this numerical simulation, with about eight elements in the transverse direction of the solid walls and twice as much in the channel thickness, are shown in Figure 6 for the same four values of the Péclet number.

Comparison of Figures 5 and 6 allow a cross-validation of both simulations since the presented temperature distributions are identical.

Sensitivity of the Temperature Distribution to the Parametrization Number of the Velocity Profile

Figures 7a and 7b shows the same profiles as above for a Péclet number $\mathrm{Pe} = 13.3$ and two values of the parametrization number K (3 and 7) using the analytical model. One clearly sees that the two distributions are quasi identical within the resolution of Figure 7, except possibly in the upstream transition region, which means that estimation of more than three velocities using the temperature distribution as input data will be difficult for this value of the Péclet number and for this excitation length.

Sensitivity to the Velocity Components

In order to see whether the estimation of three components u_k (for $k = 1$ to 3) of the velocity profile is possible, it is very useful to plot the reduced sensitivities $X_{uk} = u_k \frac{\partial T}{\partial u_k}$ of the rear and front face temperatures to these parameters. These coefficients are plotted in Figure 8a; one notices that for each face, the variation of the three sensitivities are nearly proportional over the heating length, except in the transition region, for this level of the Péclet level. The two sensitivity coefficients X_{u1} and X_{u3} are equal for the rear face signal, which means that the two velocities u_1 and u_3 cannot be estimated separately from measurements, while the three sensitivity coefficients are more independent for the front face. Figure 8b allows a closer look at this possible proportionality of the sensitivity coefficients in the upstream transition region; it confirms the superiority of front face estimation. Similar studies made for different Péclet numbers show that the higher the Péclet number is, the better the estimation of the different velocities seems to be (less dependent sensitivity coefficients).

Periodic Excitation

The study presented in the previous section has shown that transition regions seem to be the most interesting ones for estimating the velocity distribution. So, a different space dependent thermal excitation with a repetition of transition regions deserves to be studied. The front and rear face temperature responses to this type of excitation, a $q(x)$ power density composed of ten door functions, each 5 mm in length, with a $q = 4{,}000\ \mathrm{W/m^2}$ uniform intensity separated by 15-mm length gaps, are shown in Figure 9a. The plot of the sensitivity coefficients shown in Figure 9b seems to show a slight decorrelation of the front face sensitivity coefficients.

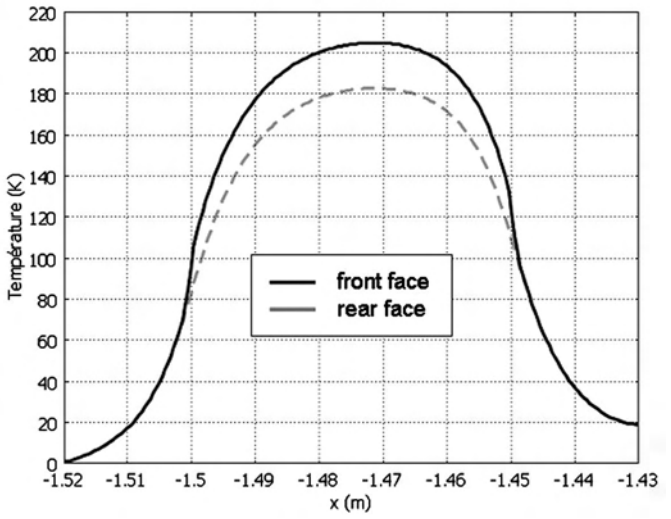

(a)

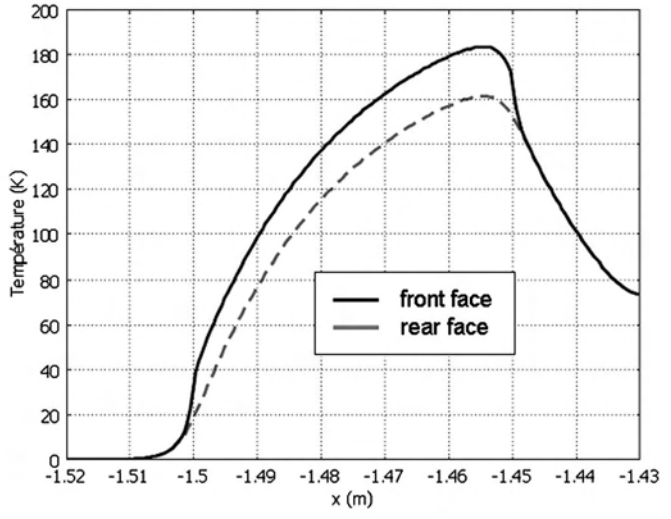

(b)

Figure 6. Effect of the Péclet number on the distribution of front and rear face temperatures (numerical model; same excitation $q = 4{,}000\ \mathrm{Wm}^{-2}$; $L_{source} = 50$ mm; velocity distribution parametrized into $K = 3$ pieces): (a) Pe = 0.133, (b) Pe = 1.33, (c) Pe = 13.3, and (d) Pe = 133. (*continued*)

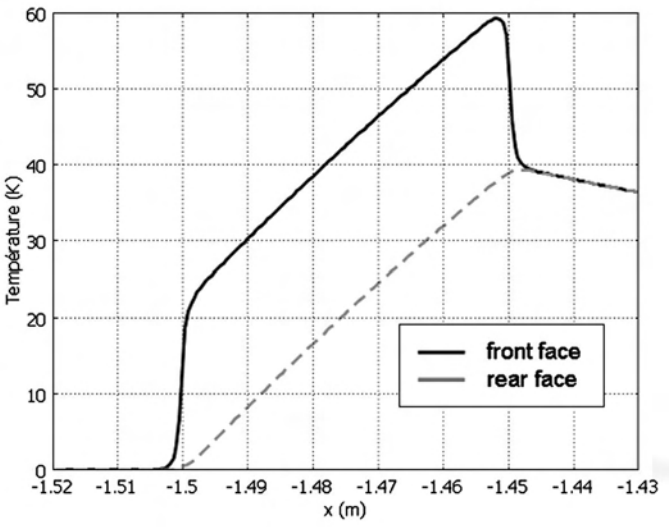

(c)

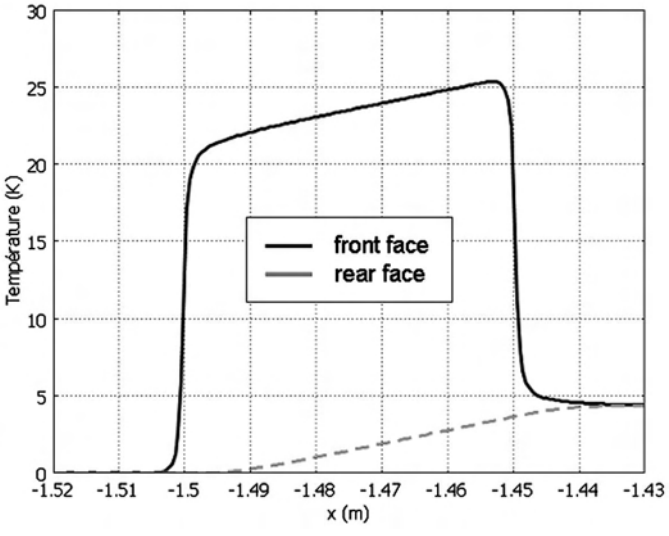

(d)

Figure 6. (*Continued*).

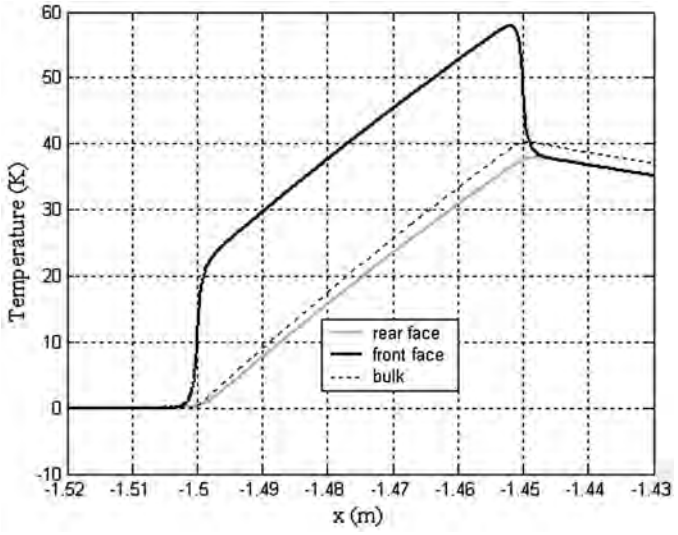

(a)

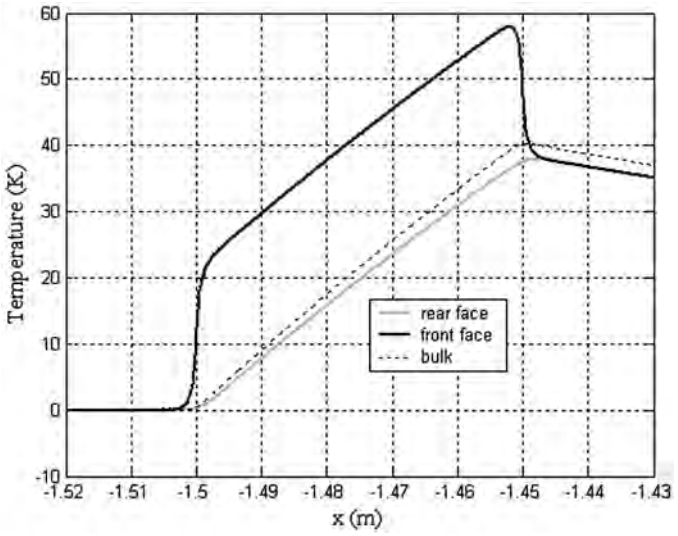

(b)

Figure 7. Effect of the number K on layers used in the parameterization of the velocity profile on the distributions of the rear and front face temperature and on the bulk temperature; Pe $=$ 13.3: (a) $K = 3$ and (b) $K = 7$.

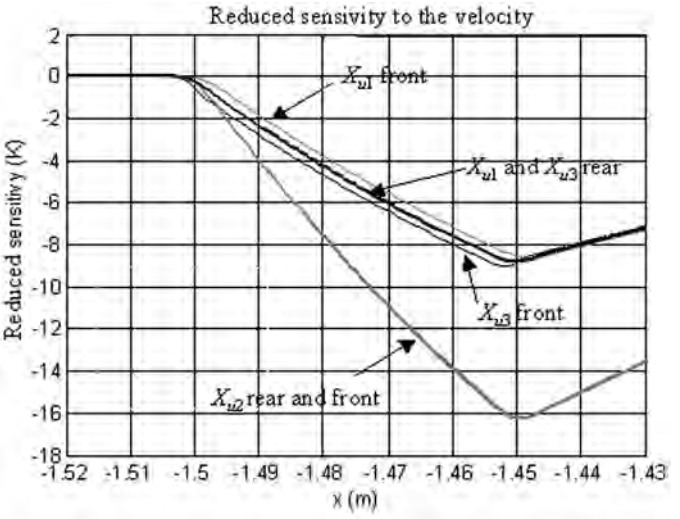

(a)

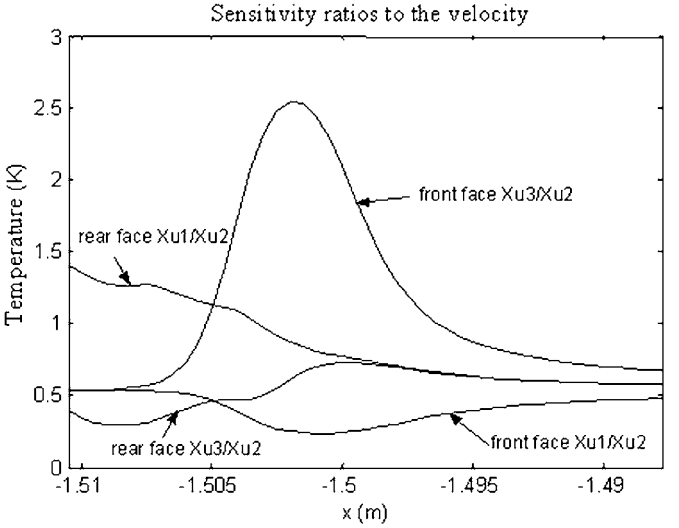

(b)

Figure 8. Door function heat power density case; $q = 4{,}000$ W.m^{-2}; Pe = 13.3: (a) reduced sensitivities to the three velocities; Pe = 13.3 and (b) ratio of reduced sensitivities; Pe = 13.3.

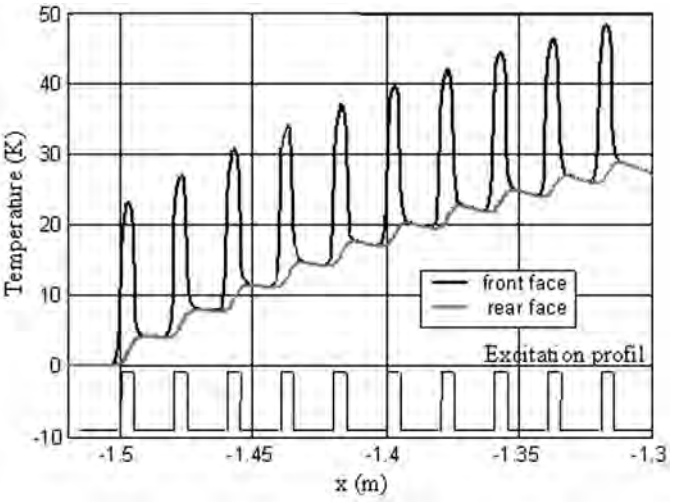

(a)

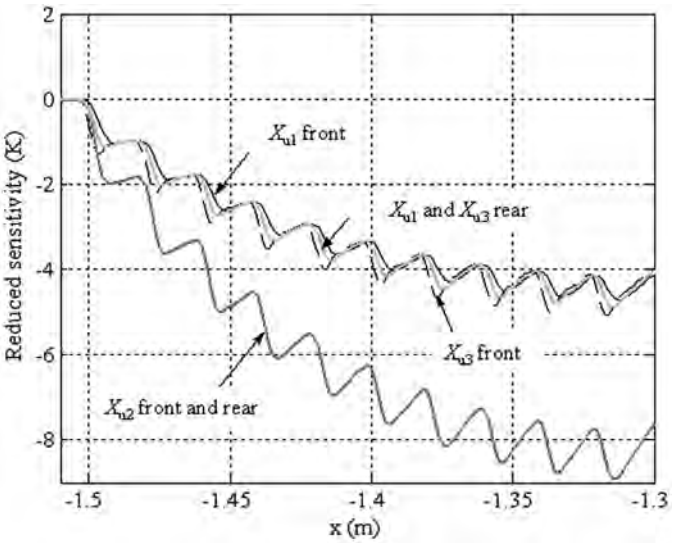

(b)

Figure 9. Periodical heat power density case; $q = 4{,}000\ \mathrm{W.m^{-2}}$; Pe = 13.3: (a) front and rear face temperature distributions and (b) front and rear face reduced sensitivities to the three velocities.

However, these two sensitivity studies in steady-state thermal regime show that estimating velocities starting from the measured external wall surface temperature field (infrared thermography) constitute a tricky task; the mean velocity can easily be reached, but retrieving the whole velocity distribution (for the highest value of the number of components K) is much more difficult, because this inverse problem becomes rather ill-posed for a value of K greater than unity.

The transient version of this problem (transient thermal excitation for a steady-state velocity distribution) will not be considered here, and the experimental implementation of this modeling will be considered now.

FIRST EXPERIMENTAL DIRECT MEASUREMENTS

The bench is composed of two polycarbonate ($\lambda_s = 0.2$ W.m^{-1}.K^{-1}) plates that form the central part of a three-layer channel of 3-mm total thickness ($e_s = 1$ mm for the walls; $e_f = 1$ mm for the flow), of $w = 50$-mm width, and of useful length $L_{channel} = 60$ mm (see Figure 10). The fluid is water flowing in a closed loop, with an inlet temperature imposed by a circulating fluid thermostat. Water enters the system through a four-inlet distributor and then flows into a tranquillization chamber. It then enters the channel and flows through two filters in order to make the temperature and velocity as uniform as possible in its useful section. The system is symmetrical if the flow direction is reversed.

The flow rate is imposed and measured thanks to a ball flowmeter. A heating resistor of length $L_{source} = 50$ mm and width w is stuck over the external face of the wall (front face). The heating power delivered by the resistor can reach 45 W.

Internal temperatures of the walls are measured through thermocouples of a K-type. An infrared camera can measure the distribution of the temperature of the rear face. This face has not been covered by any deposit, since its emissivity in the medium infrared

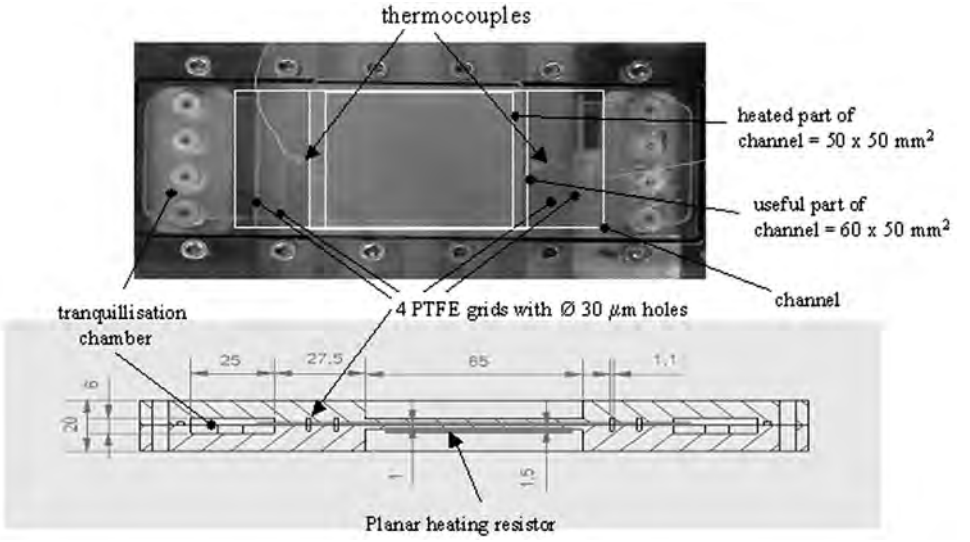

Figure 10. Realization of the mini-channel bench.

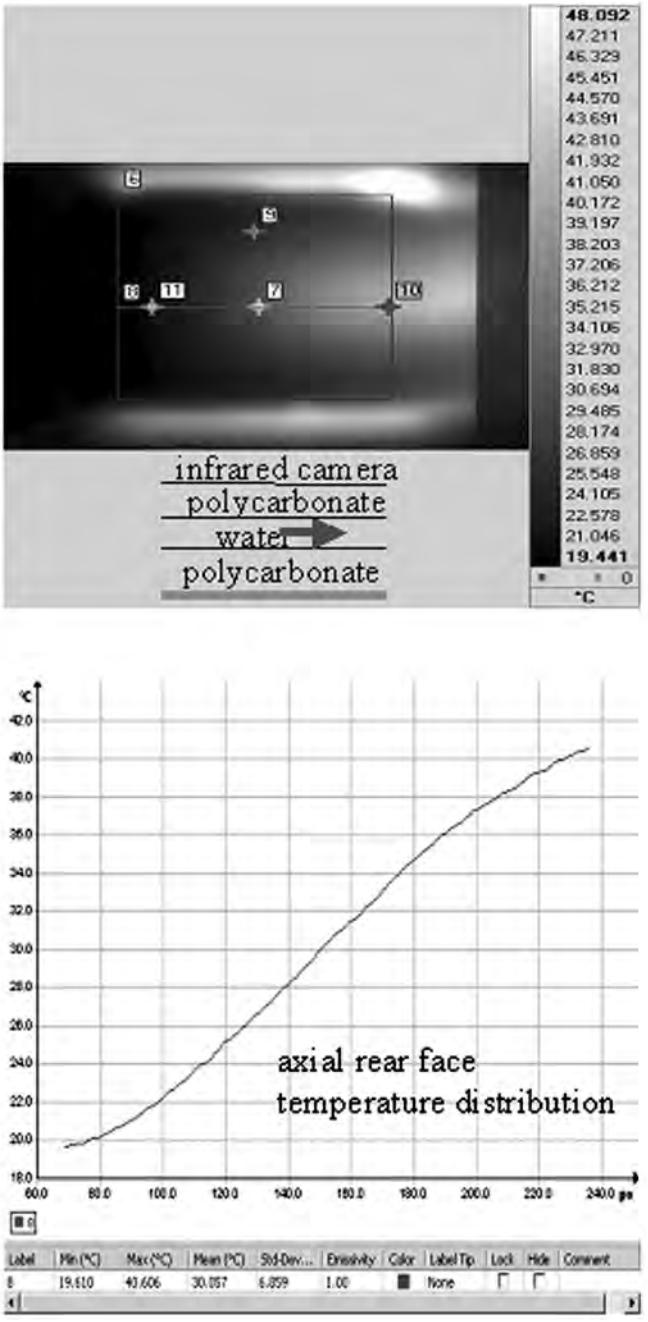

Figure 11. Infrared image and axial rear face temperature distribution.

spectral interval of the camera is high enough because of machining, which allows the detection of possible air bubbles.

A first temperature profile of the central axis of the channel (segment linking points 8, 11, 7, and 10) is shown in Figure 11. It corresponds to a mean velocity $U = 13.8$ mm/s (Pe = 183). A hot spot is visible in the upper right corner of the infrared frame above point 10; it is caused by defective adhesion of the foil resistor in that region. Future works will be made with metallic deposits instead of a glued foil resistance for thermal excitation.

CONCLUSIONS

A semi-analytical model that allows the calculation of the conjugated heat transfer inside a channel limited by two parallel walls and heated by an external planar heat source has been constructed. It does not require the use of any internal heat transfer coefficient and is based on the discretization of the velocity transverse distribution into a profile of K uniform velocities. The inverse problem based on the measurement of the temperature distribution on the external faces of the walls has been studied. It shows that information about the internal velocities is mainly present in the transition regions corresponding to the upstream and downstream ends of the heated section of the channel. First, experimental infrared temperature measurements over the channel length are presented. Future works will be devoted to electrical heating through a submicronic metallic deposit and to temperature measurements on both rear and front faces of the channel in order to get both boundary conditions of the thermal problem with maximum sensitivity to the internal velocity distribution. Other perspectives concern possible inversion of the transient temperature solution right after the start of heating and the filtration velocity characterization of the same channel filled by a porous material through which water can flow.

REFERENCES

1. G. P. Celata, Single- and Two-Phase Flow Heat Transfer in Micropipes, *Proc. 5th European Thermal-Sciences Conference Eurotherm 2008*, http://www.eurotherm2008.tue.nl/.
2. R. B. Peterson, Numerical Modeling of Conduction Effects in Microscale Counterflow Heat Exchangers, *Microscale Thermophys. Eng.*, vol. 3, pp. 17–30, 1999.
3. G. Maranzana, I. Perry, and D. Maillet, Mini and Micro-Channel: Influence of Axial Conduction in Walls, *Int. J. Heat Mass Transf.*, vol. 47, pp. 3993–4004, 2004.
4. A. Testu, S. Didierjean, D. Maillet, C. Moyne, T. Metzger, and T. Niass, Thermal Dispersion Coefficients for Water or Air Flow Through a Bed of Glass Beads, *Int. J. Heat Mass Transf.*, vol. 50, pp. 1469–1484, 2007.
5. D. Maillet, S. André, J. C. Batsale, A. Degiovanni, and C. Moyne, *Thermal Quadrupoles—Solving the Heat Equation Through Integral Transforms*, John Wiley & Sons, Ltd., Chichester, 2000.